

LETTER • OPEN ACCESS

Quasi-continuous exhaust operational space

To cite this article: M. Dunne *et al* 2024 *Nucl. Fusion* **64** 124003

View the [article online](#) for updates and enhancements.

You may also like

- [A New Method of Using Production Data to Predict the Effect of Oil Well Liquid Lifting Based on Deep Learning](#)
Shuiqingshan Lu, Chuanzhi Cui, Zhongwei Wu et al.
- [Distributing and Mapping Museums Effective Routes: A Particle Swarm Optimization Approach \(Bandung Municipality Case\)](#)
L Safriana, Nurhayati, Widiyani et al.
- [Model-predictive kinetic control with data-driven models on EAST](#)
D. Moreau, S. Wang, J.P. Qian et al.

Letter

Quasi-continuous exhaust operational space

M. Dunne^{1,*} , M. Faitsch¹ , L. Radovanovic² , E. Wolfrum¹ 
and the ASDEX Upgrade Team^a

¹ Max-Planck-Institut für Plasmaphysik, Boltzmannstr. 2, 85748 Garching, Germany

² Institute of Applied Physics, TU Wien, Fusion@ÖAW, Wiedner Hauptstr. 8-10, 1040 Vienna, Austria

E-mail: mike.dunne@ipp.mpg.de

Received 31 July 2024, revised 2 October 2024

Accepted for publication 22 October 2024

Published 1 November 2024



Abstract

The IPED predictive pedestal code has been used to determine the critical gradients for the onset of 1) separatrix ballooning modes and 2) global peeling-ballooning modes as a function of plasma shaping. This results in a scaling of the onset threshold of separatrix ballooning modes as a function of elongation and triangularity $\alpha_{\text{edge,crit}} = 0.64\kappa^{2.2}(1 + \delta)^{0.9}$, while the critical gradient for global peeling-ballooning modes increases as $\approx \alpha_{\text{edge,crit}}^{1.5}$. This implies that operational space for a ballooning unstable separatrix and stable peeling-ballooning modes exists at sufficiently high shaping. Applying a collisional broadening based scaling of the separatrix gradients allows the critical separatrix density, required to drive the separatrix ballooning mode, to be derived from global plasma parameters for any operational scenario on any device. Evaluations for ASDEX Upgrade, JET, and the ITER 15 MA baseline plasma predict critical separatrix densities of 0.3–0.4 n_{GW} for QCE access, making the QCE an attractive operational scenario for fusion devices.

Keywords: edge localised modes, MHD, peeling-ballooning, predictive, separatrix, small ELMs, quasi-continuous exhaust

(Some figures may appear in colour only in the online journal)

1. Introduction

One of the key challenges facing magnetic confinement fusion as a viable energy source is combining high temperatures (>10 keV) in the plasma center with low temperatures

(<1 eV) at the walls of device. The fall-off length of the temperature and density in these plasmas is dominated by the onset of turbulent transport. A major breakthrough in the reduction of the size of tokamak devices was obtained with the discovery of the H-mode [1]; instead of one single fall-off length extending throughout the entire confined plasma, the formation of a region of strongly reduced radial transport at the plasma edge was observed. This leads to the formation of steep temperature and density gradients in the final 5% of the enclosed plasma, with approximately one order of magnitude drop in the pressure across this region. This region of reduced transport is known as the pedestal, due to its effect of lifting the core plasma to higher temperatures and densities.

The steep gradients at the plasma edge provide free energy to a second class of instability, the large-scale

^a See Zohm *et al* 2024 (<https://doi.org/10.1088/1741-4326/ad249d>) for the ASDEX Upgrade Team.

* Author to whom any correspondence should be addressed.



Original Content from this work may be used under the terms of the [Creative Commons Attribution 4.0 licence](https://creativecommons.org/licenses/by/4.0/). Any further distribution of this work must maintain attribution to the author(s) and the title of the work, journal citation and DOI.

magnetohydrodynamic (MHD) peeling-ballooning (PB) modes [2], driven by the pressure gradient and its associated bootstrap current density in the tokamak edge. Once the linear threshold for the PB modes has been reached the mode amplitude increases exponentially on a timescale in the sub- μ s range culminating in a loss of particles and energy from the confined plasma to the open field lines and, eventually, the plasma-facing components, on a sub-millisecond time-scale. Reviews of ELM physics and a comparison of ELM classifications and potential mitigation schemes can be found in e.g. [3–5]. The problem is further amplified by the localised deposition of the power on the plasma-facing components. Once the edge gradients have been sufficiently relaxed, the cycle restarts, with particles and energy flowing into the pedestal region and restoring the transport-limited gradients in a quasi-periodic cycle. The time between the crashes of these edge-localised modes (ELMs) varies significantly, from some few milliseconds to several hundred milliseconds on larger devices.

On present-day devices, the ELM crash poses no significant danger to the longevity of plasma facing components. However, projections of the peak energy fluence from individual ELM crashes towards future devices, such as ITER, indicate that these explosive events will lead to significant damage to the plasma facing components [6]. Substantial effort has, therefore, been invested into investigating specific methods of operating tokamaks such that either no or small-ELMs occur, while keeping the core plasma hot and dense. ELM suppression via magnetic perturbation coils [7–9], the quiescent H-mode (QH-mode) [10], or the quasi-continuous exhaust (QCE) regime [11–13] integrate a manageable heat load on the plasma facing components with high pedestal top pressure as the limiting instabilities in these cases do not necessarily eject filaments from the hotter regions of the plasma. The basic strategy of these regimes is to raise the critical pressure gradient for large-scale MHD instabilities and concomitantly increase the level of transport at the plasma edge such that this critical gradient is not reached. Alternatives to H-mode operation which offer potentially similar confinement in large devices are the I-mode [14–16] and negative triangularity operation [17–20], where the H-mode and the associated ELMs are avoided entirely. While these regimes have all been robustly accessed on modern-day devices, predictive models are required in order aid the design and operational strategy of future tokamaks.

The QCE regime relies on two main access criteria; a strongly elongated and triangular poloidal plasma cross-section, and a high density at or close to the separatrix, a contour describing the last magnetic flux surface which closes on itself [12, 21, 22]; this letter will shed light on the physics behind both of these criteria. Due to the sensitivity of QCE-access on separatrix conditions, it is hypothesised that the observed filamentary transport originates there. Experimental [22] and modelling [23] work have demonstrated that QCE access is, indeed, consistent with the appearance of a ballooning mode close to the separatrix which

provides enough additional transport to prevent the global MHD modes from growing. The QCE has, however, been shown to exist close to the global threshold, indicating that the pedestal structure away from the separatrix can be well described using ideal-MHD based models. The importance of the separatrix density, rather than the pedestal top density or collisionality, makes this regime of interest for both ITER and a fusion power plant, as the separatrix density and temperature expected in these devices is comparable to what is obtained in present-day machines.

High values of plasma elongation and triangularity, as well as the presence of a second magnetic null are commonly observed access-criteria for the QCE. Despite efforts on two tokamaks, the Germany-based ASDEX Upgrade (AUG) and the Swiss Tokamak à Configuration Variable (TCV) [24], to separate the relative importance of each of these shaping parameters, no progress has been made experimentally; the parameters are all closely linked, particularly at the high-shaping employed for the QCE. In this letter we apply an MHD-based model to numerically scan the shaping parameters elongation and triangularity and determine how they impact both global and local stability. Section 2 demonstrates the stabilising effect of increased plasma shaping on peeling-ballooning and local ballooning modes, allowing space for the QCE to exist. The gradients of temperature, density, and pressure close to the separatrix are evaluated in section 3 using a collisional transport broadening approach [22, 25] which provides a minimum density for QCE access. Extrapolations to JET and ITER are made in section 4, providing input for future experiments and a promising outlook for ITER operation in the QCE regime.

2. MHD stability for shaped plasmas

The starting parameters are a 1 MA, 2.5 T AUG-sized plasma ($R_{\text{geo}} = 1.65$ m, $a_{\text{minor}} = 0.5$ m). A shaping scan has been performed using the predictive pedestal code IPED [26] where the elongation κ is varied in steps of 0.1 between 1.3 and 2.0 and the triangularity δ from -0.4 to $+0.5$, also in steps of 0.1. For each of these shaping combinations (80 in total) 11 possible pedestal profiles were constructed using the EPED 1.0 hypothesis ($\Delta_{\text{ped}} = D\sqrt{\beta_{\text{pol, ped}}}$, with $D = 0.076$). The bootstrap current in the pedestal was calculated using the Redl formula [27], with a polynomial core profile to reach the 1 MA total current. For each pedestal profile an equilibrium is calculated using the HELENA code [28] (which also calculates the $n = \infty$ local ballooning stability), followed by a global peeling-ballooning analysis using the MISHKA code [29]. Toroidal mode numbers $n = [3, 5, 7, 10, 12, 15, 20, 30, 40]$ are used in the scan.

Figure 1 illustrates the definitions used in this work. Plotted are profiles of the normalised pressure gradient α – in purple and green. For the combination $\kappa = 1.7$ and $\delta = 0.3$, the most unstable toroidal mode number from the MISHKA calculations is 5. The mode envelope for this mode is shown as the shaded green region, highlighting that this is a broad mode

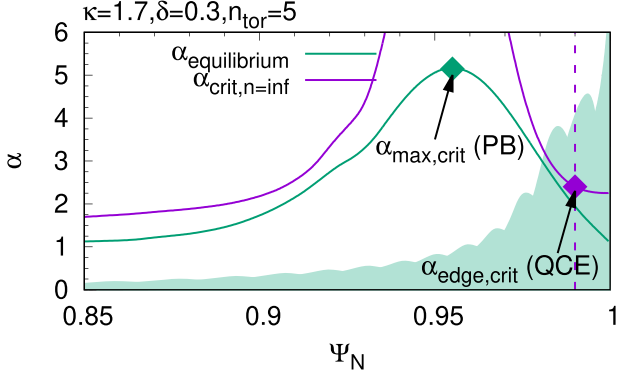


Figure 1. The equilibrium α profile (green) for the shaping combination $\kappa = 1.7$ and $\delta = 0.3$ which is unstable to global peeling-ballooning modes. The mode envelope for the $n = 5$ mode is shown as the shaded region. The α profile which is unstable at each radial location to $n = \infty$ modes is shown in purple, and the intersection of this curve with the purple dashed vertical line shows $\alpha_{\text{edge,crit}}$.

which exists over the entire pedestal; this corresponds to a ‘global’ mode (in the sense of the pedestal) which would trigger a large ELM crash. This mode is represented in the scalings later in this letter as $\alpha_{\text{max,crit}}$, marked in the plot as the green diamond (i.e. the maximum α in the pedestal), where α is the normalised pressure gradient defined as $\alpha = -\frac{2\delta_\psi V}{(2\pi)^2} \left(\frac{V}{2\pi^2 R_0}\right)^{1/2} \mu_0 p'$ [30]. This normalised pressure gradient can also be expressed in the cylindrical limit in its more intuitive form: $\alpha = -\frac{2\mu_0 R_0}{B^2} q^2 p'$, which demonstrates that α is proportional to the gradient of the local β_{poloidal} . The purple solid line shows the value of α which is unstable to $n = \infty$ modes; these are ideal modes localised to a single flux surface and act as a proxy for resistive or kinetic ballooning modes which are hypothesised to be responsible for the transport in the QCE regime. The intersection of this curve and the vertical dashed purple line, corresponding to 99% of the poloidal flux, indicates the value of $\alpha_{\text{edge,crit}}$ used in the scaling.

The α profile at the global MHD stability boundary (chosen by the criterion $\gamma_{\text{Alfven}} = 0.04$) is then taken from each shape and linear power-law regressions are performed to form scalings for:

- (i) the critical α at $\Psi_N = 0.99$ to represent the local ballooning stability near to the separatrix: $\alpha_{\text{edge,crit}} = 0.64\kappa^{2.2}(1 + \delta)^{0.9}$
- (ii) the critical α_{max} where the pedestal becomes unstable to global peeling-ballooning modes: $\alpha_{\text{max,crit}} = 0.57\kappa^{3.3}(1 + \delta)^{1.3}$.

The exponents indicate the ordering of elongation vs triangularity in terms of pedestal stability; elongation has a higher exponent, demonstrating that this is the leading order effect for stabilisation of both global peeling-ballooning modes and local ballooning modes. More interestingly, since both critical alphas scale differently with elongation and triangularity,

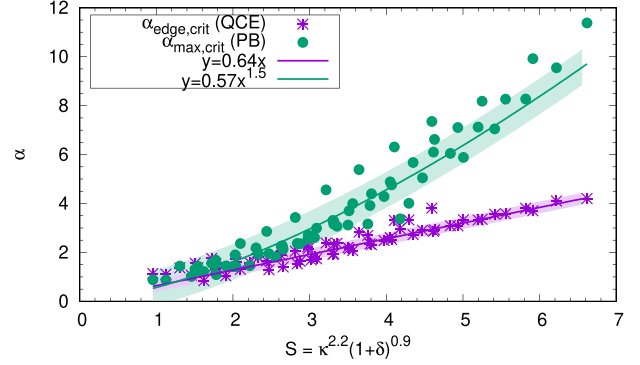


Figure 2. Critical α for global PB modes (green) and local ballooning modes (purple) as a function of shaping. The shaded areas indicate the range which includes 90% of the solutions at a given shaping parameter.

this suggests that an operational space exists where the pressure gradient close to the separatrix is high enough to create the transport required for the QCE, but allowing the global PB mode to remain stable. Based on the scaling of the local ballooning $\alpha_{\text{edge,crit}}$, we define a generalised shaping parameter $S = \kappa^{2.2}(1 + \delta)^{0.9}$ as an ordering parameter in the following.

The proposed operational space is visualised in figure 2. The critical α for global peeling-ballooning modes (green) according to the MISHKA calculations ($\alpha_{\text{crit,PB}}$) and for local ballooning modes (purple), calculated by HELENA, ($\alpha_{\text{edge,crit}}$) are plotted as a function of the shaping parameter. By definition, the local ballooning $\alpha_{\text{edge,crit}}$ increases linearly while $\alpha_{\text{crit,PB}}$ scales roughly as $\alpha_{\text{edge,crit}}^{1.5}$. From the figure it is clear that the possibility for separation between the local and global instabilities occurs at a shaping parameter of 3; this would correspond to e.g. $\kappa \approx 1.6$ and $\delta \approx 0.1$, typical values for a weakly shaped plasma. A more clear separation occurs at a shaping parameter of ≈ 4 , corresponding to e.g. $\kappa \approx 1.65$ and $\delta \approx 0.35$, typical values for QCE plasmas at AUG.

These results demonstrate for the first time the physics of why high shaping, particularly high elongation, is required in order to access QCE. Should the experimental α close to the separatrix meet the requirement for both local and global modes, then the QCE cannot dominate the transport and some form of global mode can occur; this may also be in the form of resistive MHD modes which are suspected to limit the pedestal to low α_{max} at JET [31]. As the shaping is increased, the threshold for a global instability to occur increases faster than the threshold for a separatrix-localised instability.

Despite the opening of the operational space shown here, it cannot be excluded that further parameters, e.g. closeness-to-double-null, which can influence local and global stability, are also important for the existence of the QCE. For example, a scan in squareness (the next shaping moment after triangularity, which we have not shown in this letter) has shown that $\alpha_{\text{edge,crit}}$ can be affected without a large impact on the threshold for peeling-ballooning modes. Note that this model proposes high shaping as a minimum requirement for the QCE. For example, at a shaping parameter of 4, $\alpha_{\text{max,crit}}$ and $\alpha_{\text{edge,crit}}$

are approximately 5 and 2, respectively. If the edge ballooning mode is not driven unstable (see the next section), then the pedestal could reasonably be expected to grow to obtain an α_{\max} of 5 and a large ELM would be triggered. We assume in this work that the transport caused by the separatrix ballooning mode is sufficient to prevent this. The critical edge density to drive this mode unstable is derived in the next section, providing an exact criterion for QCE-access.

3. Separatrix density condition

The second well-known parameter for access to the QCE is high separatrix density which increases the pressure gradient close to the separatrix [21] and provides the drive for the local ballooning mode. Here, we compare this with our calculated $\alpha_{\text{edge,crit}}$. We follow the methodology used by Eich [25, 32] and Faitsch [22] to determine the electron temperature at the edge (classified as one folding length inside of the last closed flux surface), $T_{e,\text{edge}}$, via Spitzer–Harm conductivity and the pressure fall-off length, λ_p , from a collisional-broadening based description of gradient length in the edge. The main focus in this work is on the scalings given in [22] as this was based on a data set of highly shaped AUG discharges (the Eich-scalings are based on discharges with lower shaping). The temperature and pressure fall-off lengths are given by:

$$\lambda_T = 2.57 (1 + 0.38\alpha_t^{3.3}) \rho_{s,\text{pol}} \quad (1)$$

$$\lambda_p = 1.55 (1 + 0.61\alpha_t^{2.35}) \rho_{s,\text{pol}} \quad (2)$$

where $\rho_{s,\text{pol}}$ is the ion poloidal Larmor radius and α_t is defined as

$$\alpha_t = 3.13 \times 10^{-18} R_0 q_{\text{cyl}}^2 \frac{n_{e,\text{edge}} Z_{\text{eff}}}{T_{e,\text{edge}}} \quad (3)$$

with R_0 the geometrical major radius, $q_{\text{cyl}} = \frac{B_T \kappa_{\text{eff}}}{B_\theta A}$ the equivalent cylindrical edge safety factor, $\kappa_{\text{eff}} = \sqrt{(1 + \kappa^2 \times (1 + 2\delta^2 - 1.2\delta^3))/2}$ and A the aspect ratio. With these definitions, and specified values for the power crossing the separatrix P_{sep} , the plasma shape, q -profile, Z_{eff} , and separatrix density, the separatrix temperature and the gradient lengths can be calculated in an iterative manner. For a standard ASDEX Upgrade case, we assume a P_{sep} of 7 MW, typical for well-heated AUG discharges, but the result is only weakly dependent on this value, and a Z_{eff} of 1.3. To demonstrate the impact of the edge density on the predicted operational space of the QCE, we have run a predictive pedestal simulation using a real AUG shape (in contrast to the analytic shapes discussed above). We have chosen a 1 MA/2.5 T plasma scenario and a range of separatrix densities up to 50% of the Greenwald density. For each separatrix density, we have calculated $T_{e,\text{edge}}$, λ_T , λ_p , combined these with the local q -profile (as opposed to the q_{cyl} value used in the scalings) and formed α_{edge} , the expected experimental edge normalised pressure gradient, which can be compared to $\alpha_{\text{edge,crit}}$.

The results of this example are shown in figure 3. The various α parameters are plotted as a function of the separatrix density. While some change of $\alpha_{\text{edge,crit}}$ (dashed purple)

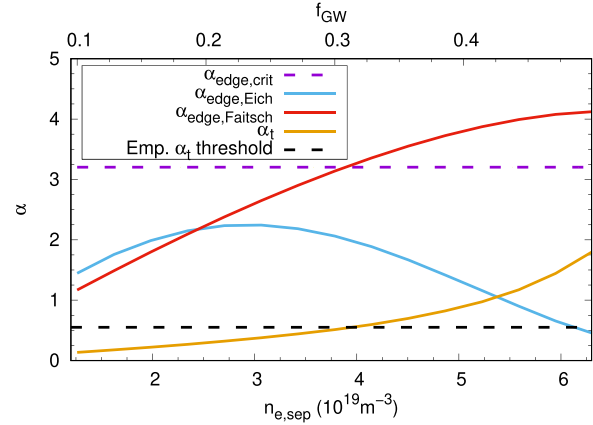


Figure 3. Critical α values (purple: $\alpha_{\text{edge,crit}}$, black: $\alpha_{t,\text{crit}}$), α_t (yellow), and projected α_{edge} from the Eich (blue) and Faitsch (red) scalings.

with increasing density may be expected, this is not taken into account in this scan and it remains constant. The α value related to the PB stability, $\alpha_{\max,\text{crit}}$, is not shown in this figure and assumed to be high enough that, once the edge ballooning mode is unstable, no large ELM will be triggered.

The figure shows the expected α_{edge} values from both the Eich (blue) and Faitsch (red) edge operational-space scalings, as well as the collisional transport parameter α_t (yellow); also sketched for reference is the empirical small-ELM threshold [22] of $\alpha_t = 0.55$ (dashed black). Owing to its strong α_t dependence, the Eich scaling predicts that the pressure gradient will never reach $\alpha_{\text{edge,crit}}$. However, the Faitsch scaling results in an α_{edge} which exceeds $\alpha_{\text{edge,crit}}$ at an edge density of $4 \times 10^{19} \text{ m}^{-3}$. The key difference between the two scalings originates in the pre-factor of the α_t broadening, which is higher in the Eich-scaling; this is likely linked to the plasma shaping using in the respective data-sets, with higher shaping in the QCE data set resulting in a higher threshold for α_t broadening. Coincidentally, the density at which $\alpha_{\text{edge,Faitsch}}$ reaches $\alpha_{\text{edge,crit}}$ corresponds to an expected α_t of 0.55, the empirical threshold, making these theories impossible to separate in this particular example.

The combination of the global and local stability limits and the collisional broadening-inspired gradient scaling has resulted in an intuitive model model which demonstrates the experimentally observed access conditions for the QCE. High plasma shaping stabilises both the global and separatrix-localised modes, but acts more strongly on the global modes. The model also shows that increasing the separatrix density acts a drive for the separatrix ballooning modes and we can derive a minimum $n_{e,\text{sep}}$ for QCE access, which we will now apply to other devices.

4. Extrapolation to other devices

The model presented in the previous sections requires, for the most part, only engineering parameters to determine if access to the QCE regime is possible. The exception are the global β and pedestal top density required for the peeling-ballooning

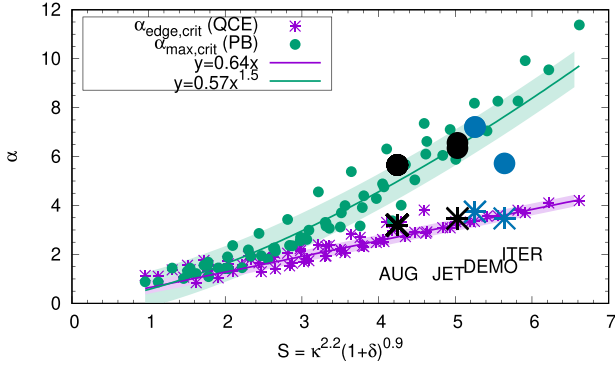


Figure 4. Critical alphas vs shaping parameter for AUG and JET (black), and ITER and EU-DEMO (blue) operational scenarios overlaid on the model data set; $\alpha_{\text{edge,crit}}$ and $\alpha_{\text{max,crit}}$ vary only slightly with changes in q_{95} , density, and global β .

calculations and Z_{eff} required for both the peeling-ballooning and α_{edge} calculations. Bearing this in mind, it is possible to investigate access to the QCE for different devices. Figure 4 shows additional points overlaid on figure 1. These points are calculated for JET, ITER and EU-DEMO. A range of combinations of I_p and B_T have been used for JET, with $\beta_N = 2.0$, $n_{e,\text{ped}} = 70\%n_{\text{GW}}$ and a double null plasma shape. The full-current ITER-baseline operational scenario has been chosen for ITER (15 MA, 5.3 T, $\beta_N = 1.8$, $n_{e,\text{ped}} = 8 \times 10^{19} \text{ m}^{-3}$) and a high-current EU-DEMO scenario has been taken (18 MA, 5.6 T, $\beta_N = 2.8$, $n_{e,\text{ped}} = 6 \times 10^{19} \text{ m}^{-3}$). Black (AUG and JET) and blue (ITER and EU-DEMO) circles are the calculated peeling-ballooning limit for the three devices while the black and blue stars are the critical α at $\Psi_N = 0.99$. Despite the differences in q , β_N , density, machine size, and the use of the ‘real’ shapes (cut at $\Psi_N = 0.994$)³, the critical alphas for these three devices overlap closely with those from the shaping parameter scan, validating the generality of the trends. In particular, due to the high shaping, all three devices appear to have the capacity to access QCE. As we will see later in the case of ITER, the QCE is predicted to be a default operational regime.

4.1. The QCE at JET

To investigate the QCE access in terms of the separatrix density, we perform the analysis from section 3 for two promising JET scenarios by scanning the density at the separatrix. Two examples are shown in figure 5; (a) a 1.5 MA/2.3 T scenario and (b) a 2.0 MA/2.8 T scenario. As in figure 3 the main focus is the intersection of the dashed purple ($\alpha_{\text{edge,crit}}$) and solid red ($\alpha_{\text{edge,Faitsu}}$) lines, predicting the critical edge density for QCE access in these scenarios. The critical density scales approximately with plasma current, occurring at ca. 40% n_{GW} in both cases.

³ This is not expected to impact the stability of either the separatrix ballooning or global peeling-ballooning modes significantly, as the cut-off value typically only impacts the growth rate of pure peeling-modes.

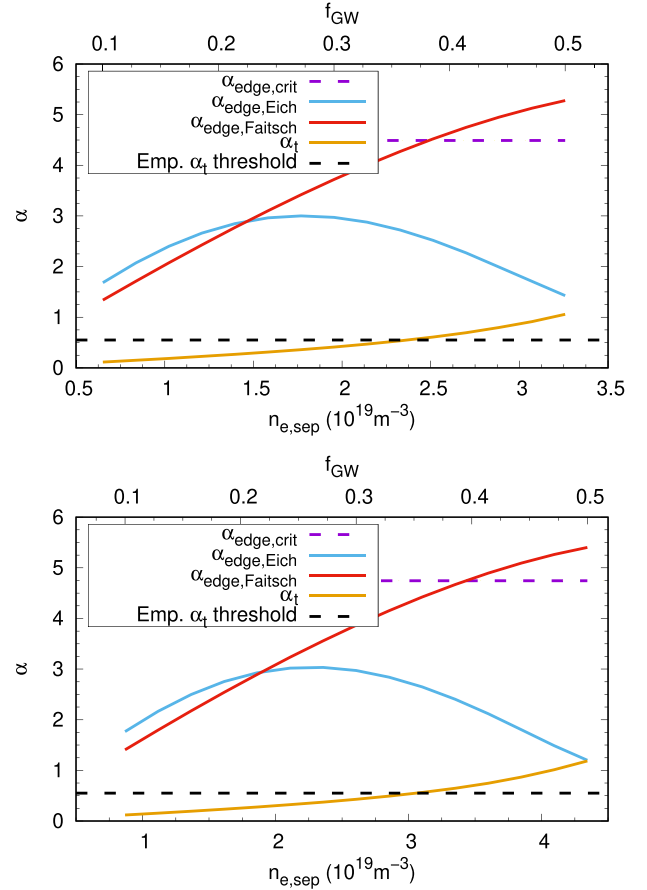


Figure 5. α vs $n_{e,\text{sep}}$ for (a) 1.5 MA/2.3 T and (b) 2.0 MA/2.8 T scenarios at JET using a close-to-double null shape. The color scheme is the same as in figure 3. QCE access is predicted in both scenarios at a relatively high separatrix density of ca. 40% n_{GW} .

Scans of P_{sep} and $Z_{\text{eff,sep}}$ show that scenarios with the highest heating power and lowest $Z_{\text{eff,sep}}$ have the highest likelihood to enter QCE and do so at lower $n_{e,\text{sep}}$. This makes JET-ILW a better candidate for QCE access compared to e.g. JET-C, due to the lower expected $Z_{\text{eff,sep}}$.

4.2. Extrapolation to ITER

The same procedure has been applied to the ITER-baseline scenario with a range of P_{sep} [60, 80, 100, 120] MW and $Z_{\text{eff,sep}}$ [1.3, 1.8, 2.0] values. α_{edge} is plotted as the black lines as a function of $n_{e,\text{sep}}$ in figure 6 with the purple line showing $\alpha_{\text{edge,crit}}$; for all possible combinations of P_{sep} and $Z_{\text{eff,sep}}$ robust QCE access is predicted with the peeling ballooning boundary expected at $\alpha_{\text{PB,crit}} = 6.0$ for this scenario. The minimum density required to access QCE in this scenario corresponds to approximately 30% of the Greenwald density, which should be readily achievable in ITER; this fraction is notably lower than expected for e.g. JET, but in line with the expectations for AUG (figure 3). As a simple extended investigation, we assume that once $\alpha_{\text{edge,crit}}$ has been reached λ_p and, hence, also λ_q , will increase with increasing $n_{e,\text{sep}}$ to maintain α_{edge} at its critical value, mirroring the expected increase in transport in the QCE. The $\lambda_{p,\text{crit}}$ is calculated by simply inverting the

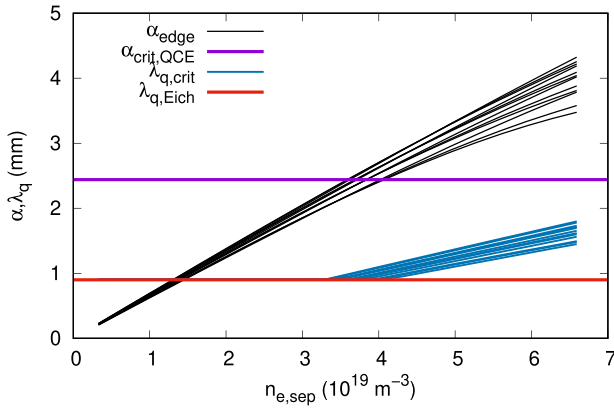


Figure 6. α_{edge} (black) plotted as a function of $n_{e,\text{sep}}$ for a range of power and Z_{eff} values for ITER. The purple line denotes $\alpha_{\text{edge,crit}}$. The projected inter-ELM λ_q is shown as the red line and simple SOL broadening from the QCE as the blue lines, increasing once the QCE is entered.

α_{edge} calculation and setting $\alpha_{\text{edge}} = \alpha_{\text{edge,crit}}$; a self-consistent re-evaluation of the temperature and density with the increased λ_q has not been performed. $\lambda_{q,\text{OMP}}$ is calculated as described in [22] and plotted as the blue lines where it exceeds the Eich scaling for this scenario (0.9 mm), plotted as the red line. This indicates that, in addition to QCE access in ITER being quite likely, it should also correspond to increased power fall-off lengths in the near-SOL. The situation is qualitatively similar for a fusion reactor; the high poloidal field and P_{sep} lead to high values of α_{edge} , enabling access to the QCE. If the transport from the QCE is sufficient, this would also act as a mechanism to increase the power fall-off length in the near-SOL.

5. Conclusions

In this letter we have presented a novel predictive model for access to the QCE scenario based on a combination of global- and local-MHD and separatrix transport. Criteria for the minimum shaping, defined as a combination of elongation and triangularity, $S_d = \kappa^{2.2}(1 + \delta)^{0.9}$, and the separatrix density have been defined, explaining the main experimentally observed ingredients for QCE access and agreeing well with AUG observations. The key ingredient defining the shaping is the opening of operational space for the separatrix gradient to become unstable before a global mode can be triggered; this principle can be extended to other ELM-free scenarios, where a range of modes, either MHD or turbulent in nature, dominate transport. While a first-principles transport model has not been employed in this work, the scalings for the separatrix gradients in temperature and pressure derived using a collisional broadening ansatz are expected to reflect the leading-order physical processes.





Using this model, predictions for JET, ITER and EU-DEMO have been made. QCE access is expected at JET in the two scenarios examined, with high P_{sep} and low $Z_{\text{eff,sep}}$ giving the highest access probability. Previous attempts to obtain this regime at JET may have been hampered by the higher Z_{eff}

at the separatrix and a total shaping slightly lower than that used in AUG. Experimental work on JET (or JT-60SA) can validate these predictions in a large device while non-linear modelling can verify the level of transport which can be expected in this scenario and if it is, indeed, sufficient to avoid the occurrence of large explosive edge localised modes ELMs and extend the near-SOL fall-off lengths. Due to the combination of high P_{sep} and short gradient-lengths (coming from the high poloidal field) QCE access in ITER, by the criteria discussed here, is projected to be quite likely, resulting in a promising outlook for the ELM-free operation of this and other future fusion devices.

Acknowledgments

This work has been carried out within the framework of the EUROfusion Consortium, funded by the European Union via the Euratom Research and Training Programme (Grant Agreement No. 101052200—EUROfusion). Views and opinions expressed are however those of the author(s) only and do not necessarily reflect those of the European Union or the European Commission. Neither the European Union nor the European Commission can be held responsible for them. Lidija Radovanovic is a fellow of the Friedrich Schiedel Foundation for Energy Technology.

ORCID iDs

M. Dunne  <https://orcid.org/0000-0002-5259-9970>
M. Faitsch  <https://orcid.org/0000-0002-9809-7490>
L. Radovanovic  <https://orcid.org/0000-0002-1311-0482>
E. Wolfrum  <https://orcid.org/0000-0002-6645-6882>

References

- [1] Wagner F. *et al* 1982 Regime of improved confinement and high beta in neutral beam heated divertor discharges of the ASDEX tokamak *Phys. Rev. Lett.* **49** 1408–12
- [2] Wilson H.R., Cowley S.C., Kirk A. and Snyder P.B. 2006 Magneto-hydrodynamic stability of the H-mode transport barrier as a model for edge localized modes: an overview *Plasma Phys. Control. Fusion* **48** A71–A84
- [3] Zohm H. 1996 Edge localized modes (ELMs) *Plasma Phys. Control. Fusion* **38** 105
- [4] Leonard A.W. 2014 Edge-localized-modes in tokamaks *Phys. Plasmas* **21** 090501
- [5] Ham C., Kirk A., Pamela S. and Wilson H. 2020 Filamentary plasma eruptions and their control on the route to fusion energy *Nat. Rev. Phys.* **2** 159–67
- [6] Eich T., Sieglin B., Thornton A.J., Faitsch M., Kirk A., Herrmann A. and Suttrop W. 2017 ELM divertor peak energy fluence scaling to ITER with data from JET, MAST and ASDEX Upgrade *Nucl. Mater. Energy* **12** 84–90
- [7] Evans T.E. *et al* 2006 Edge stability and transport control with resonant magnetic perturbations in collisionless tokamak plasmas *Nat. Phys.* **2** 419–23
- [8] Suttrop W. *et al* 2018 Experimental conditions to suppress edge localised modes by magnetic perturbations in the ASDEX Upgrade tokamak *Nucl. Fusion* **58** 096031

- [9] Hu Q.M. *et al* 2021 Predicting operational windows of ELMs suppression by resonant magnetic perturbations in the DIII-D and KSTAR tokamaks *Phys. Plasmas* **28** 052505
- [10] Burrell K.H. *et al* 2002 Quiescent H-mode plasmas in the DIII-D tokamak *Plasma Phys. Control. Fusion* **44** A253–63
- [11] Stober J., Maraschek M., Conway G.D., Gruber O., Herrmann A., Sips A.C.C., Treutterer W. and Zohm H. (ASDEX Upgrade Team) 2001 Type-II ELMy H-modes on ASDEX Upgrade with good confinement at high density *Nucl. Fusion* **41** 1123–34
- [12] Wolfrum E. *et al* 2011 Characterization of edge profiles and fluctuations in discharges with Type-II and nitrogen-mitigated edge localized modes in ASDEX Upgrade *Plasma Phys. Control. Fusion* **53** 085026
- [13] Faitsch M., Eich T., Harrer G.F., Wolfrum E., Brida D., David P., Griener M. and Stroth U. 2021 Broadening of the power fall-off length in a high density, high confinement H-mode regime in ASDEX Upgrade *Nucl. Mater. Energy* **26** 100890
- [14] Hubbard A.E. *et al* 2017 Physics and performance of the I-mode regime over an expanded operating space on Alcator C-Mod *Nucl. Fusion* **57** 126039
- [15] Happel T. *et al* 2019 Stationarity of I-mode operation and I-mode divertor heat fluxes on the ASDEX Upgrade tokamak *Nucl. Mater. Energy* **18** 159–65
- [16] Liu Y.J. *et al* 2020 Power threshold and confinement of the I-mode in the EAST tokamak *Nucl. Fusion* **60** 082003
- [17] Austin M.E. *et al* 2019 Achievement of reactor-relevant performance in negative triangularity shape in the DIII-D tokamak *Phys. Rev. Lett.* **122** 115001
- [18] Paz-Soldan C. *et al* 2021 Plasma performance and operational space without ELMs in DIII-D *Plasma Phys. Control. Fusion* **63** 083001
- [19] Coda S. *et al* 2021 Enhanced confinement in diverted negative-triangularity L-mode plasmas in TCV *Plasma Phys. Control. Fusion* **64** 014004
- [20] Nelson A.O., Schmitz L., Paz-Soldan C., Thome K., Cote T., Leuthold N., Scotti F., Austin M., Hyatt A. and Osborne T. 2023 Robust avoidance of edge-localized modes alongside gradient formation in the negative triangularity tokamak edge *Phys. Rev. Lett.* **131** 195101
- [21] Harrer G.F. *et al* 2018 Parameter dependences of small edge localized modes (ELMs) *Nucl. Fusion* **58** 112001
- [22] Faitsch M., Eich T., Harrer G.F., Wolfrum E., Brida D., David P., Dunne M., Gil L., Labit B. and Stroth U. 2023 Analysis and expansion of the quasi-continuous exhaust (QCE) regime in ASDEX Upgrade *Nucl. Fusion* **63** 076013
- [23] Radovanovic L., Dunne M., Wolfrum E., Harrer G., Faitsch M., Fischer R. and Aumayr F. 2022 Developing a physics understanding of the quasi-continuous exhaust regime: pedestal profile and ballooning stability analysis *Nucl. Fusion* **62** 086004
- [24] Labit B. *et al* 2019 Dependence on plasma shape and plasma fueling for small edge-localized mode regimes in TCV and ASDEX Upgrade *Nucl. Fusion* **59** 086020
- [25] Eich T., Manz P., Goldston R.J., Hennequin P., David P., Faitsch M., Kurzan B., Sieglin B. and Wolfrum E. 2020 Turbulence driven widening of the near-SOL power width in ASDEX Upgrade H-Mode discharges *Nucl. Fusion* **60** 056016
- [26] Dunne M.G. *et al* 2017 Global performance enhancements via pedestal optimisation on ASDEX Upgrade *Plasma Phys. Control. Fusion* **59** 025010
- [27] Redl A., Angioni C., Belli E. and Sauter O. 2021 A new set of analytical formulae for the computation of the bootstrap current and the neoclassical conductivity in tokamaks *Phys. Plasmas* **28** 022502
- [28] Huysmans G.T.A., Goedbloed J.P. and Kerner W. 1991 Isoparametric bicubic hermit elements for solution of the Grad-Shafranov equation *Int. J. Mod. Phys. C* **02** 371
- [29] Mikhailovskii A.B. 1998 Generalized MHD for numerical stability analysis of high-performance plasmas in tokamaks *Plasma Phys. Control. Fusion* **40** 1907–20
- [30] Miller R.L., Chu M.S., Greene J.M., Lin-Liu Y.R. and Waltz R.E. 1998 Noncircular, finite aspect ratio, local equilibrium model *Phys. Plasmas* **5** 973–8
- [31] Frassinetti L. *et al* 2021 Role of the separatrix density in the pedestal performance in deuterium low triangularity JET-ILW plasmas and comparison with JET-C *Nucl. Fusion* **61** 126054
- [32] Eich T. and Manz P. (ASDEX Upgrade Team) 2021 The separatrix operational space of ASDEX Upgrade due to interchange-drift-Alfvén turbulence *Nucl. Fusion* **61** 086017